Guiding centre, full gyromotion, and fast-ion losses in stellarators

P. Rodrigues[1], M. Assunção[1], E. Gomes[1], J. Ferreira[1], and R. Jorge[2]

[1]*Instituto de Plasmas e Fusão Nuclear, Instituto Superior Técnico, Universidade de Lisboa, 1049-001 Lisboa, Portugal.*

[2]*Department of Physics, University of Wisconsin-Madison, Madison, Wisconsin 53706, USA.*

Unlike tokamaks, stellarators must have their 3D magnetic field accurately optimised in order to confine charged particles long enough to achieve sustainable fusion reactions. Fast ions with energy significantly above the thermal fuel, produced by the heating systems or by fusion reactions, are particularly challenging because their large gyro-radius may compare with localised spatial features of the field. One way to achieve this confinement goal is to optimise stellarator magnetic fields regarding omnigenity, a geometric property that provides a sufficient condition for particle confinement. Quite recently, omnigenous stellarator magnetic configurations were obtained with outstanding accuracy levels, either quasisymmetric [1] or quasi-isodynamic [2]. Following an alternative approach, optimised configurations were also produced by direct estimates of particle losses via guiding-centre trajectories [3].

In this work, we show that the fraction of lost alpha-particles computed with a full-gyromotion algorithm is substantially larger than the one obtained under the guiding-centre approximation for some of these optimised configurations. Other configurations, however, are more resilient regarding losses but the predicted fraction of particles that manage to drift away from their original magnetic surface is always larger if a full-gyromotion approach is employed when compared with the guiding-centre approximation.

In order to proceed, three sets of recently proposed stellarator magnetic-fields configurations are considered, all rescaled to the size of the `ARIES-CS` reactor design [4] (i.e., same minor radius and volume-averaged field). The field components $B^i(\psi,\phi,\theta)$ and the map from flux coordinates (normalised toroidal flux ψ and the angles ϕ,θ along each magnetic surface) to the cartesian space are computed by the MHD equilibrium code `VMEC` [5]. Suitable radial resolution and spectral content is kept to ensure numerical $\nabla\cdot\mathbf{B}$ values sufficiently close to zero.

The first set (Fig. 1, top) was obtained by requiring precise quasisymmetry [1], that is, optimising the field magnitude $B(\psi, m\vartheta - n\zeta)$ to depend on a linear combination of the Boozer angles ϑ,ζ. This ensures a third guiding-centre motion invariant, besides energy and magnetic moment, and thus limits the particle's radial drift. Two cases are tested: one with quasiaxisymmetry (QA, $n=0$) and the other with quasihelical (QH) symmetry. The second set (Fig. 1, middle), provides examples of quasi-isodynamic (QI) configurations [2], where the field $\mathbf{B}(\psi,\vartheta,\zeta)$ follows geometric constraints (other than Boozer-angle symmetry) that force the bounce average of the guiding-centre radial drift to vanish. Cases with 1, 2, and 3 field periods are tested. The third set departs entirely from geometric concepts and the field was instead optimised to minimise the α-particle lost fraction as evaluated by directly following the guiding-centre motion of a marker ensemble (with size $\sim 10^3$) for up to 10 msec [3]. Two cases were produced

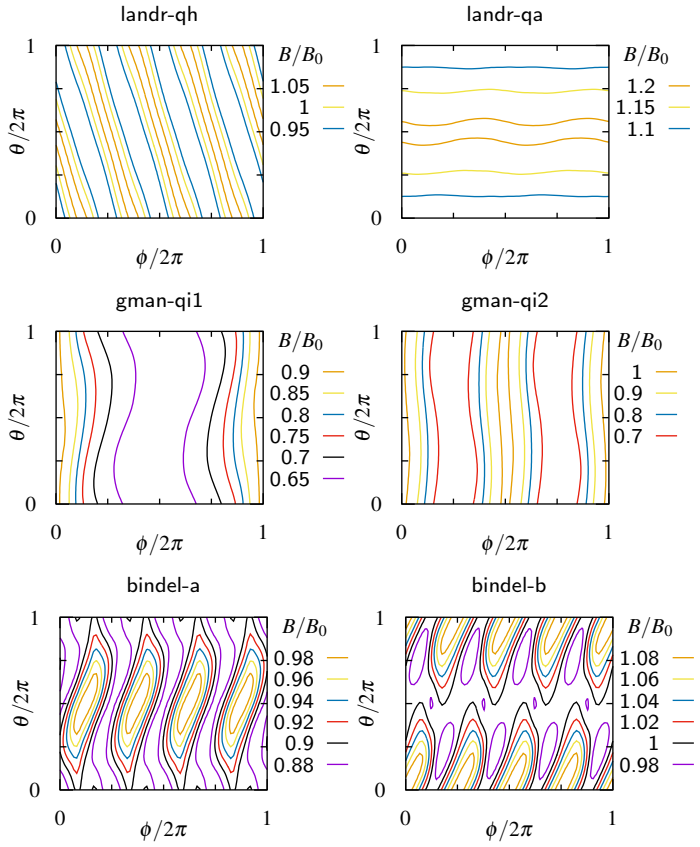

Figure 1: Contours of the field magnitude at the surface $\psi = 0.25$ for each configuration.

with different strategies for particle initialisation, one over the surface $\psi = 0.25$ (a) and the other across the full plasma volume (b) [3].

For each of the optimised stellarator configurations listed above, two populations of markers (with size 5×10^4) are followed for 10 msec, one within the GC approximation and the other keeping a FG description. FG particle tracing employs the Boris algorithm [6] to advance the markers (charge q_s and mass m_s) according to the Lorentz force (no electric field, $\partial_t \mathbf{B} = 0$), i.e.,

$$\dot{q}^k = v^k, \quad \dot{v}^k = -\Gamma^k_{ij} v^i v^j + \frac{q_s}{m_s}\big(\mathbf{v}\times\mathbf{B}\big)^k \tag{1}$$

where q^k are general curvilinear coordinates (in our case, the flux coordinates). In turn, GC tracing employs a 4-th order Runge-Kutta algorithm to integrate the drift equations [7]

$$\eta\,\dot{Q}^k = \tilde{v}_\parallel b^k + \tilde{\Omega}^{-1}\left[\tilde{v}_\parallel^2 \tilde{\nabla}\times\mathbf{b} + \mathbf{b}\times\mathbf{d}\right]^k, \quad \eta\,\dot{\tilde{v}}_\parallel = -\mathbf{d}\cdot\left(\mathbf{b} + \tilde{v}_\parallel \tilde{\Omega}^{-1}\tilde{\nabla}\times\mathbf{b}\right) \tag{2}$$

for the GC position and parallel velocity, with $\mathbf{b} = \mathbf{B}/B$, $\eta = 1 + \tilde{v}_\parallel \tilde{\Omega}^{-1}\mathbf{b}\cdot\tilde{\nabla}\times\mathbf{b}$, $\mathbf{d} = \frac{1}{2}\tilde{\mu}\tilde{\nabla}\tilde{B}$, and the tilde denoting normalisation to a reference length $L_{\rm ref}$, velocity $v_{\rm ref}$, or time $L_{\rm ref}/v_{\rm ref}$. Numerical integration tools are implemented over `gyronimo` [8], a gyromotion library taking care of most differential-geometry algebra (coordinate transformations, metric tensors, etc) that has already seen use on particle tracing for optimised stellarators [9].

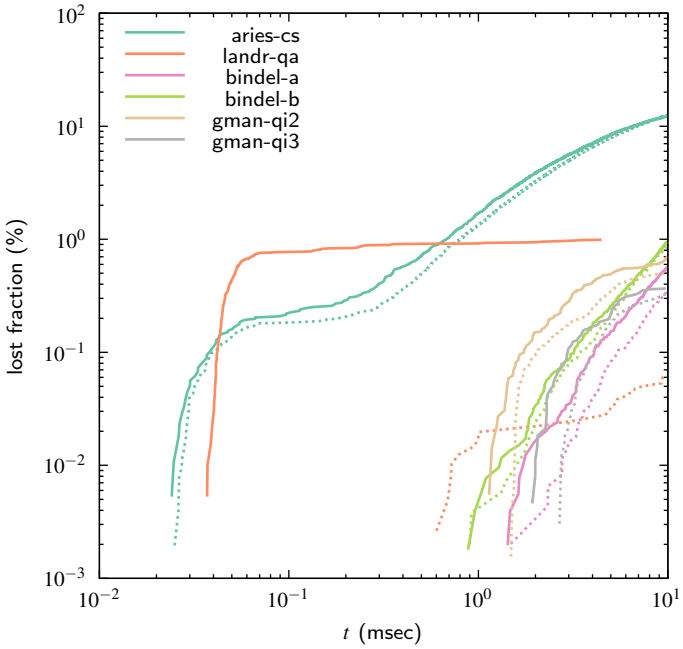

Figure 2: Accumulated lost fraction (FG in solid lines, GC in dotted lines) as a function of time.

The isotropic α-particles population produced at a single magnetic surface ($\psi = 0.25$) by DT reactions ($E = 3.5$ MeV) is simulated by a distribution of markers with randomly initialised angles $0 \leq \phi, \theta < 2\pi$ and pitch $-1 \leq \lambda = v_{\|}/v \leq 1$. A random gyrophase is also needed for FG tracing. The time step size Δt corresponds to about 1 (GC) and 100 (FG) samples per gyration. The latter value is a compromise between the better accuracy provided by smaller Δt and the concomitant larger error induced by the cartesian-to-flux coordinate transformation that Boris algorithm requires at an increasing number of time steps.

The simulation results are plotted in Fig. 2, where the `ARIES-CS` case is also represented for comparison. Quite strikingly, there are no predicted losses up to the 10 msec limit, either by FG or GC, for some particular configurations (landr-qh and gman-qi1). For the other cases, the losses predicted by FG are always larger than GC ones, in most cases by a factor up to $\sim 60\%$. Notwithstanding, some specific configurations seem to be resilient regarding FG effects (bindel-b and aries-cs), with similar lost fractions being predicted in both approaches. In turn, the QA case (landr-qa) is quite remarkable, as predicted FG losses exceed GC ones by one order of magnitude. Also, the former begin to take place one order of magnitude earlier than the latter.

A closer analysis shows that the loss characteristics of the QA case are determined by the significantly large orbit width allowed. On one hand, it favours prompt losses (i.e., in less than one bounce period), accounting for their early beginning. One such FG example is shown in Fig. 3. On the other hand, the same argument should apply to GC orbits, which is clearly not the case. The cause is also evident in Fig. 3, where the corresponding GC orbit lies within one

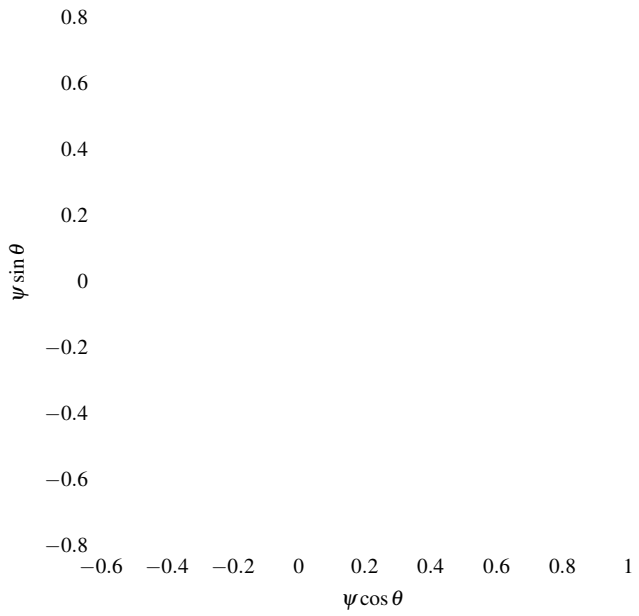

Figure 3: Prompt-loss orbit (blue, FG in dots, GC in lines) and final bounce period of a delayed-loss orbit (green) in QA; Largest-width orbits in QH (purple) and QI (orange) cases.

gyro-radius from the edge, being thus classified as confined. Indeed, GC orbits require several bounce periods in order to slowly drift towards the edge (delayed losses). Conversely, the typical orbit width in the lossless QH and QI cases is significantly smaller (Fig. 3).

In summary, optimised configurations were found to respond differently to FG effects on their confinement properties, whose impact may reach up to one order of magnitude. These results suggest the importance of a more detailed confinement analysis after the optimisation stage.

Acknowledgments

IPFN activities were supported by FCT - Fundação para a Ciência e Tecnologia, I.P. by project UIDB/50010/2020 and DOI identifier 10.54499/UIDB/50010/2020 (https://doi.org/10.54499/UIDB/50010/2020), project UIDP/50010/2020 and DOI identifier DOI 10.54499/UIDP/50010/2020 (https://doi.org/10.54499/UIDP/50010/2020) and project LA/P/0061/202 and DOI 10.54499/LA/P/0061/2020 (https://doi.org/10.54499/LA/P/0061/2020).

References

[1] M. Landreman and E. Paul, Phys. Rev. Lett. **128**, 035001 (2022).
[2] A. Goodman et al., J. Plasma Phys. **89**, 905890504 (2023).
[3] D. Bindel et al., Plasma Phys. Control. Fusion **65** 065012 (2023).
[4] F. Najmabadi et al., Fusion Sci. Technol. **54**, 655 (2008).
[5] S. Hirshman et al., Phys. Fluids **26**, 3553 (1983).
[6] H. Qin et al., Phys. Plasmas **20**, 084503 (2013).
[7] R. G. Littlejohn, J. Plasma Physics **29**, 111 (1983).
[8] P. Rodrigues et al., "`gyronimo`: an object-oriented library for gyromotion applications", 49th EPS conference on plasma physics, Bordeaux (2023); `github.com/prodrigs/gyronimo`
[9] P. Figueiredo et al., J. Plasma Phys. **90**, 905900207 (2024).